Available online at www.sciencedirect.com

SCIENCE DIRECT

Thin Solid Films 485 (2005) 218 – 223

www.elsevier.com/locate/tsf

# Micromagnetic studies of iron microbars prepared by nanoimprint lithography and electrodeposition

Darko Grujicic, Batric Pesic*

*University of Idaho, College of Engineering, Department of Materials Science and Engineering, McClure Hall, Moscow, ID 83844-3024, USA*

Received 25 August 2004; accepted in revised form 24 March 2005
Available online 17 May 2005

**Abstract**

Micromagnetic and macromagnetic switching properties of iron microbars produced by electrodeposition into voids patterned by nanoimprint lithography were investigated. The study was focused on microbars with six different aspect ratios. Magnetization along the long axis produced single-domain states in all microbars regardless of their aspect ratio. In the remanent state, magnetization in microbars with smaller aspect ratios resumed the closed magnetic flux configuration. Closed magnetic flux configuration was also found in demagnetized microbars. Individual, as well as the net remanence curves, were extracted from magnetic force microscopy images to verify their agreement with the macroscopic magnetization measurements.
© 2005 Elsevier B.V. All rights reserved.

*PACS:* 75.50.Bb; 75.75.+a; 82.45.Mp
*Keywords:* Electrodeposition; Iron; Magnetic properties and measurements; Micromagnetic modeling

## 1. Introduction

Small ferromagnetic structures have recently received great attention because of their application in non-volatile magnetic random access memory (MRAM) elements [1], and because they are well suited for the studies of single domain magnetization reversal phenomena. Thin acicular iron elements [2–5], as well as ellipses and dots [5–7], were among the various shapes whose magnetization switching properties were investigated. The most commonly used deposition methods in the micromagnetic studies were e-beam evaporation [3,4,6], molecular beam epitaxy [5], or dc magnetron sputtering [7]. No record was found regarding electrodeposition of iron microbars.

This paper describes the results from the study of micromagnetic (magnetic force microscopy—MFM) and macromagnetic (vibrating sample magnetometry—VSM) properties of iron microbars with round corners. Iron microbars were produced by electrodeposition into voids patterned by nanoimprint lithography. The main investigated parameter was the effect of aspect ratio on the stability of single domain magnetization.

## 2. Experimental details

Iron microbars were produced by a procedure that involved nanoimprint lithography (Obducat, NIL 2.5 in.-Model) and electrochemical deposition. In the first step, a digital versatile disc (DVD) stamp was impressed into a polymethylmethacrylate (PMMA) layer spun on a (100) silicon wafer with a 50 nm sputtered copper seed layer. Upon reactive ion etching (Axic, HF8 MultiMode) of the excess PMMA to expose the underlying copper film, iron was electrodeposited into patterned voids. The solution containing 0.05 M $FeSO_4$ and 0.5 M $H_3BO_3$, with no other additives present, was adjusted to investigated pH (2 and 3.5). Electrodeposition was carried out at −1300 mV vs. Ag/AgCl reference electrode ($E_h^0$=+0.222 V). The DVD stamp used for patterning contained microbars with six

* Corresponding author. Tel.: +1 208 885 6569; fax: +1 208 885 2855.
*E-mail address:* pesic@uidaho.edu (B. Pesic).

0040-6090/$ - see front matter © 2005 Elsevier B.V. All rights reserved.
doi:10.1016/j.tsf.2005.03.042

length-to-width aspect ratios (AR): 1.43; 2.14; 2.86, 3.57, 4.26 and 5.00. The width of all microbars, as measured by atomic force microscopy (AFM; Digital Instruments, Nanoscope IIIa) was 650 nm. Separation between the individual microbars was at least 1000 nm in all directions.

Remanent magnetization curves were extracted from the MFM images, which were acquired in the lift mode with CoCr coated silicon tips, at the lift-height of 35 nm. Each $40 \times 40$ μm image encompassed more than 300 microbars of various aspect ratios.

## 3. Results and discussion

### 3.1. Effect of solution pH: microbars vs. nanowires

The pH of as-prepared solution containing 0.05 M $FeSO_4$ and 0.5 M $H_3BO_3$ was 3.5. According to Fig. 1a, electrodeposition from pH 3.5 solution resulted in formation of well-defined microbars that conformed to the imprinted patterns in the PMMA template. The MFM image in Fig. 1b indicates that the magnetization of as-deposited microbars form multiple domains in order to minimize the magnetostatic energy by the closure of magnetic flux.

When the solution pH was reduced to pH 2 by addition of dilute sulfuric acid, there was a dramatic change in the morphology of electrodeposited iron, as shown in Fig. 2a. Electrodeposited iron nucleated primarily along the edges of the imprinted patterns, forming closed-loop nanowires instead of planar microbars. The width of the nanowire walls was less than 100 nm, while the height of the edges was between 15 nm and 60 nm. The morphology change from microbars to closed-loop nanowires consequently resulted in different magnetization, as shown in the MFM image in Fig. 2b. The images of nanowires with sharper resolution show sections of strong dark-to-bright contrasts at the points of discontinuity (if the nanowires are not fully physically closed). This configuration corresponds to a "C" type of magnetization, where the strong divergence component of the magnetic field due to the opposing poles results in the observed contrast, while the remainder of the wire has no divergence component and produces only a weak contrast effect. A closer examination of the MFM image in Fig. 2b also shows the chirality of "C" magnetization in nanowires, distinguished again according to dark-to-bright contrasts, see arrow marks with clockwise and counter-clockwise orientation. Chiral nature of magnetization in the electrodeposited nanowires bears a great significance for the data storage application, where two different magnetization orientations could be utilized for storing the binary information.

### 3.2. Effect of aspect ratio on switching field distribution—MFM remanent magnetization curves

The effect of shape anisotropy on the switching properties of iron microbars was examined as follows. First, a sample was subjected to a magnetic field, parallel to the long axis of microbars, of $+4.7 \cdot 10^4$ A·m$^{-1}$. The field was then reversed to a certain $H_{rev}$ value and subsequently shut off. Thus prepared sample was in a remanent magnetization state, and as such transferred to MFM for imaging and construction of remanent magnetization curves. A detailed method of extracting the remanent magnetization curves from MFM images is described elsewhere [8].

According to Fig. 3a–b, a fraction of AR 1.43 and AR 2.14 microbars was always found in a demagnetized state in the investigated range of reverse fields. After the field reversal to $-4.7 \cdot 10^4$A·m$^{-1}$, only about 15% of AR 1.43 microbars were in a single-domain state at the remanence,

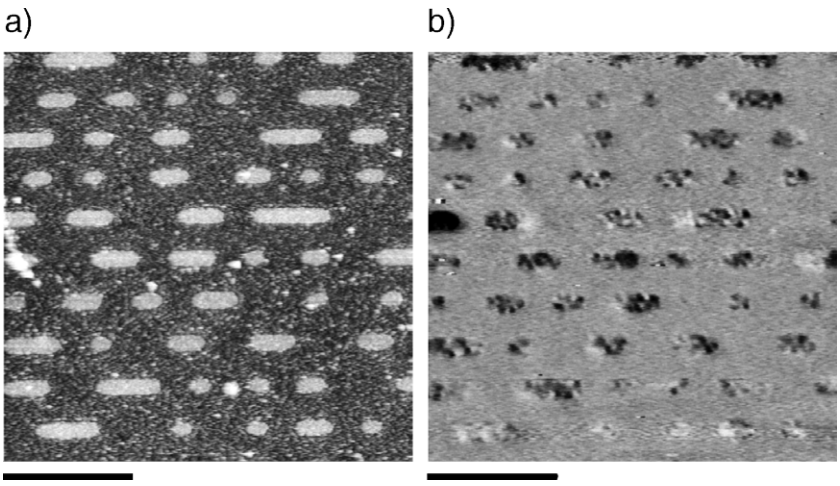


Fig. 1. a–b. a) AFM height image of iron microbars electrodeposited from solution at pH 3.5, and b) corresponding MFM frequency image in as-deposited state. Note the multi-domain magnetizations include all microbars in the figure. MFM image in b represents the frequency modulation of the oscillating CoCr cantilever, acquired while scanning 35 nm above the sample in the interleave mode. Scale bar 5 μm, vertical scale: 200 nm for AFM image, 3 Hz for MFM.

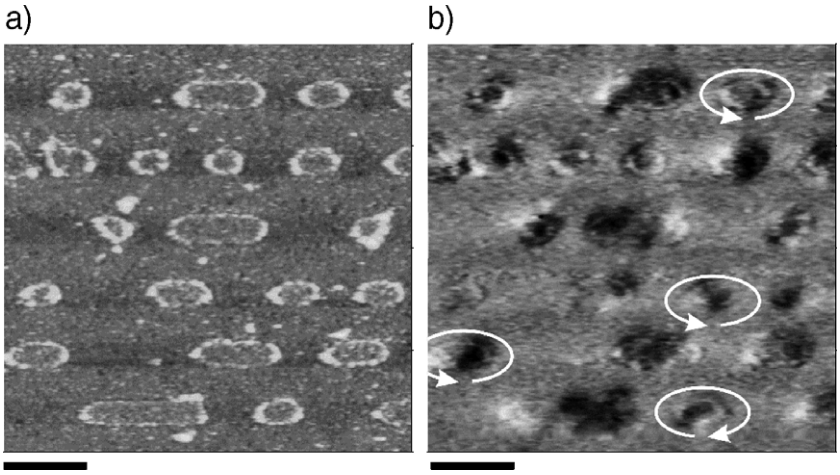


Fig. 2. a–b. a) AFM height image of iron closed-loop nanowires electrodeposited from solution at pH 2, and b) corresponding MFM frequency image in as-deposited state. Lift height 35 nm, scale bar 2 μm, vertical scale: 200 nm for AFM image, 3 Hz for MFM image.

Fig. 3a, compared to about 50% for microbars with AR 2.14, Fig. 3b. Microbars with AR 2.14 were characterized by a step in the remanence curve between $-7.96 \cdot 10^3$ A·m$^{-1}$ and $-1.59 \cdot 10^4$ A·m$^{-1}$. The step represents a region of multidomain stabilization, and was observed earlier in the remanence curves of cobalt [8] and permalloy [9] microbars, but not in nickel microbars [10].

Microbars with aspect ratio 2.86 and higher show a complete magnetization reversal in the investigated range of reversal fields. The multidomain stabilization step also appears in the remanence curves of microbars with higher aspect ratios, 2.86 to 4.26, Fig. 3c–e, but its breadth decreases with the AR increase, and finally disappears for the remanence curve with the AR 5.00. Also, the width of switching field narrows as the AR increases.

### 3.3. Switching field distribution and stability of demagnetized states

According to Fig. 3a–f, the width of switching field distribution depends on the aspect ratio of microbars. In order to determine the distribution of switching fields, the

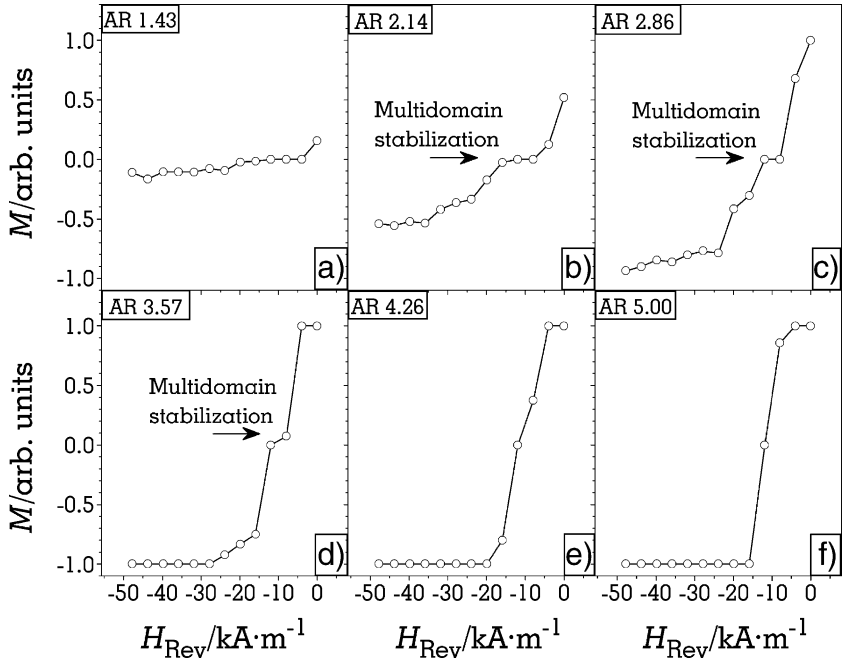


Fig. 3. a–f. Remanent curves extracted from the MFM images corresponding to iron microbars with the following length-to-width aspect ratios: a) 1.43, b) 2.14, c) 2.86, d) 3.57, e) 4.26 and f) 5.00. Open circles represent experimental data, connected by straight lines. Note that the microbars with the two smallest aspect ratios were not fully saturated in the investigated range of reversal fields. For microbars with higher aspect ratios, the width of the switching field range decreased with the increase of aspect ratio. Note also stabilization of the demagnetized states, manifested as a step or a kink on the graphs for all microbars except for those with AR 5.00.

data in Fig. 3b–f were differentiated with respect to the applied field and fitted with Gaussian distributions. Two standard deviations ($2\sigma$) of the switching field distribution were then determined from the full width at half-maximum (FWHM) of the peak on the d$M$/d$H$ curve, Fig. 4, for each aspect ratio. For the curves that exhibit two peaks, the two standard deviations were calculated from the width of both peaks combined.

In Fig. 4, the d$M$/d$H$ curves corresponding to AR 2.14, 2.86 and 3.57 microbars show two peaks, indicating the transition through a demagnetized state. As the aspect ratio increases, the positions of two peaks shift closer to each other, until the peaks finally converge into a single peak for the AR 5.00 microbars. The single peaks are centered at about $-1.2\cdot10^4$ A·m$^{-1}$, which is slightly higher than the coercivity of the bulk sample, $-8.76\cdot10^3$ A·m$^{-1}$. The appearance of the second peak signifies the stabilization of multidomain states, while the first peak corresponds to their disappearance [8,9]. Fig. 4 shows that the stabilization of multidomain states in iron microbars decreases with the aspect ratio increase, as is expected, because higher shape anisotropy (microbars with higher aspect ratios) favors single domain magnetization.

The remanent magnetization curves calculated from the MFM study were compared to the remanent magnetization curve measured for the entire sample by the VSM bulk magnetization and remanent magnetization measurements. A detailed explanation of the construction of the MFM remanent curve corresponding to the entire sample is given elsewhere [8]. The contributions from microbars with different AR are normalized with respect to their volumes.

According to the results presented in Fig. 5, there is a very good agreement between the MFM and VSM remanent

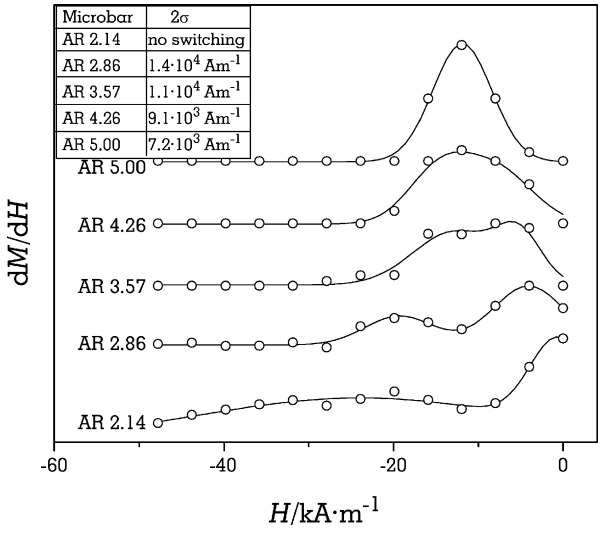


Fig. 4. d$M$/d$H$ of curves in Fig. 3b–f as a function of reversal field. The lines are Gaussian fits of the derivatives of the data in Fig. 3b–f. Note the presence of two peaks on the curves for microbars with lower aspect ratios, which converge to a single peak as the aspect ratio increases.

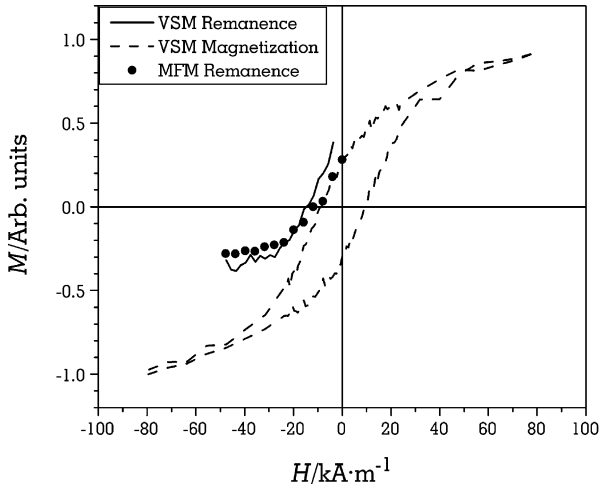


Fig. 5. The net MFM remanent magnetization curve (solid circles) compared to the VSM remanent magnetization curve (solid line) and the VSM magnetization curve (dashed line). The VSM magnetization curve was obtained by measuring magnetization while sweeping the field parallel to the sample surface in the ($+7.96\cdot10^4$ A·m$^{-1}$, $-7.96\cdot10^4$ A·m$^{-1}$) Oe range. The MFM curve was normalized with respect to the total number of iron microbars in one image, while VSM curves were normalized with respect to the saturation magnetization determined from the VSM magnetization curve.

magnetization curves in the entire investigated range of fields. The agreement between the measured and calculated remanent curves validates the use of MFM images for calculation of remanent magnetization curves for microbars of various aspect ratios, as given in Fig. 3a–f.

Another parameter of interest was the magnetization state of microbars at the nominal coercive field of $-1.2\cdot10^4$ A·m$^{-1}$. The MFM image, acquired at the remanence after magnetization to $+4.7\cdot10^4$ A·m$^{-1}$ and applied reversal field of $-1.2\cdot10^4$ A·m$^{-1}$, shows that all microbars were in a demagnetized state, regardless of the aspect ratio. Even the few longer microbars that appeared to be in a single domain state, actually consisted of several domains. In the previous studies of cobalt [8] and nickel [10], there were always microbars with the highest aspect ratio that were still in a single domain state, which was not the case with iron microbars. One reason for the absence of single domain state could be that the long axis of iron microbars was parallel to the magnetocrystalline hard axis [5]. However, because of the polycrystalline nature and the lack of epitaxy between *fcc* copper and *bcc* iron [11–13], this explanation seems unlikely.

A more plausible explanation for the absence of single domain state microbars is a high degree of magnetic interactions between the discrete elements in the deposited array. In order to estimate the effect of magnetic interactions between the microbars in the remanent state, the magnitude of the magnetic fields of microbars was calculated for a microbar with AR 5.00. Because the distances between the microbars were comparable to their lengths, the axial and lateral dipole fields were calculated according to Eqs. (1) and (2) [14]. The fields were

calculated by approximating an AR 5.00 microbar with a dipole of 3.25 μm length:

$$H_{II} = \frac{2\,prl}{\left(r^2 - \frac{l^2}{4}\right)^2} \quad (1)$$

$$H_{\perp} = \frac{pl}{\left(r^2 + \frac{l^2}{4}\right)^{\frac{3}{2}}} \quad (2)$$

where: $p$—pole strength (=$Mhw$); $M$—saturation magnetization (emu $cm^{-3}$); $l$, $h$ and $w$—length, height and width of a microbar (cm); and $r$—distance from the center of the microbar to a point in which the field is calculated (cm). According to the calculations, the axial and lateral fields at a distance of 1 μm were $3.74 \cdot 10^3$ A·$m^{-1}$ and $1.83 \cdot 10^3$ A·$m^{-1}$, respectively. Although these fields are lower than the measured coercivity of the microbars (between $7.96 \cdot 10^3$ A·$m^{-1}$ and $1.2 \cdot 10^4$ A·$m^{-1}$), it could be possible that the addition of fields from all individual microbars becomes significant enough to cause magnetic interactions at the remanence.

The calculation of magnetostatic interactions between individual microbars is possible only if the entire sample is accounted for, because of the random axial and lateral distributions of microbars of various sizes. However, because of the way the tracks are written, the microbars are aligned in pseudo-chains along their long axes, which allows for comparison with the studies related to magnetic interactions between nanowires in parallel arrays [15], and between magnetic elements in periodic arrays [2,16–19]. The deviation from the ideal, non-interacting case in Henkel plots was taken as the evidence for magnetostatic interactions in Ni–Cu/Cu nanowire arrays, in a study conducted by Robinson and Schwarzacher [15]. The evidence of magnetostatic interactions between the ferromagnetic elements in periodic arrays similar to the ones investigated here was found in studies by Kirk et al. [2], Wei and Chou [16], Grimsditch et al. [17] and Natali et al. [18]. The origins of magnetostatic interactions are related to the quadratic anisotropy of the square array of dots [18], the dot shape [17] and the dipolar coupling between the neighboring elements [2,16]. The stabilization of single domain states in elongated microbars through antiferromagnetic dipolar coupling between neighboring microbars can explain the sigmoidal shape of the magnetization curve in Fig. 5. Strong fields of both polarity may arise due to dipole–dipole interactions perpendicular to the applied field. Consequently, high saturation fields are required to align all of the microbars in one direction.

The effect of magnetic interactions on the magnetization of iron microbars is also evident in Fig. 3a–f, where a step in remanent magnetization curves that corresponds to stabilization of demagnetized states exists for microbars with AR 2.14–4.26. The same step was present only for AR 2.14 and AR 2.86 cobalt microbars [8], while it was absent in nickel microbars [10]. Decrease in the extent of stabilization of demagnetized states in microbars coincides with the decreasing magnetic moments of the elements that they were made of ($M_{\text{iron}} > M_{\text{cobalt}} > M_{\text{nickel}}$). The extent of magnetic interactions between iron, cobalt and nickel microbars therefore decreases in the same order.

Toward further understanding of the magnetization switching mechanisms, an iron microbar of AR 5.00 was selected for micromagnetic simulation utilizing the code developed by the M. Donahue and D. Porter from the National Institute of Standards and Technology [20]. The saturation magnetization used for modeling was $M_s = 1.7 \cdot 10^6$ A·$m^{-1}$, with a cell size of 10 nm × 10nm × 55 nm (film thickness). The magnetocrystalline anisotropy coefficient, $K_1$, was set to zero, implying the polycrystalline nature of microbars. The exchange stiffness parameter $A$ was set to $21 \cdot 10^{-12}$ J $m^{-1}$, while the damping coefficient $\alpha$ was set to 0.1. Simulations were stopped when the residual torque fulfilled the condition: $|\vec{m} \times \vec{H}| < 10^{-16}$. The template shape used for modeling was an actual AFM image of an AR 5.00 microbar with some edge roughness and oval corners with slight irregularities. Each cell used for calculation encompassed a template area of $5 \times 5$ pixels. The results of micromagnetic modeling are presented in Fig. 6, along with three characteristic magnetization configurations.

The simulation indicates that the magnetization reversal is initiated by the formation of vortex cores at the edges of the microbar. The reversal then proceeds through a multidomain configuration characterized by two cross-tie type walls parallel to the longer axis of the microbar. Cross-tie

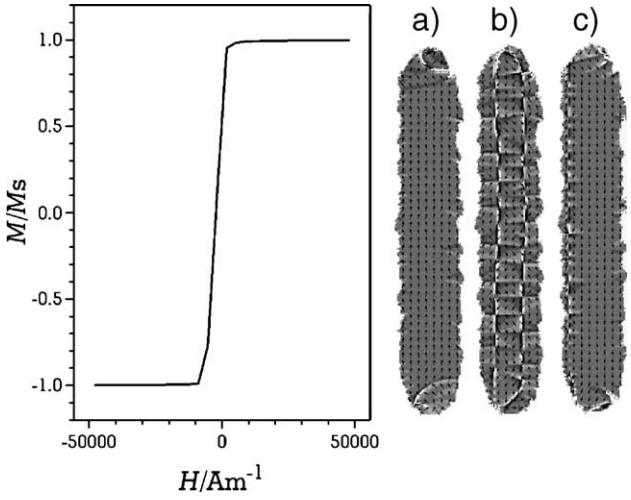


Fig. 6. Simulated magnetization curve for an AR 5.00 microbar. Simulated MFM images represent characteristic magnetization configurations at a) $+1.75 \cdot 10^3$ A·$m^{-1}$, b) $-1.75 \cdot 10^3$ A·$m^{-1}$ and c) $-5.33 \cdot 10^3$ A·$m^{-1}$, while the arrows represent directions of magnetization vectors within the microbar. The vertical scale of the simulated images is $8 \cdot 10^5$ A·$m^{-1}$.

walls have previously been reported in iron films grown on GaAs [21]. The coercivity of the simulated AR 5.00 microbar was $-2.4\cdot10^3$ A·m$^{-1}$, which was lower than the actual coercivity of $-1.2\cdot10^4$ A·m$^{-1}$. The increase of coercivity with the decrease in separation between ferromagnetic elements, due to magnetic interactions in an array, was also observed in the study of Wei and Chou [16]. Accordingly, the difference in coercivities of an isolated microbar and that in an array of microbars indicates the presence of magnetic interactions within the array of iron elements.

## 4. Conclusion

The combination of nanoimprint lithography and electrodeposition represents a very effective method for fabrication of metal microbars of various length-to-width aspect ratios. In the as-deposited state, iron microbars were found either in vortex or multidomain magnetic configurations. In an externally applied field, the magnetization configurations changed to a single-domain state.

The established correlation between the width of the switching field range and the shape anisotropy, which is a function of length-to-width aspect ratio, shows the single domain stabilization with the increase of aspect ratio. However, the single domain state was absent when the microbars were subjected to the coercive field because of quadratic anisotropy and dipole–dipole magnetostatic interactions.

There is a good agreement between the remanent magnetization curves obtained by micromagnetic analysis (MFM) and macromagnetic characterization (VSM). Micromagnetic modeling revealed that magnetization reversal takes place through vortex generation at the edges, and formation of a multidomain configuration. The difference in coercivity, between measured (MFM remanent curve) and calculated (micromagnetic model) values, indicates that the microbars in an array of ferromagnetic elements are affected by magnetostatic interactions.

## Acknowledgements

This work was sponsored by the U.S. Department of Defense, Department of the Navy, Office of Naval Research, Grant Number N000140110829, and The National Science Foundation RII Award (EPS 0132626). Help by Obducat (Malmo, Sweden) during acquisition of nanoimprint equipment and technical training is greatly appreciated.

## References

[1] G.A. Prinz, Science 282 (1998) 1660.
[2] K.J. Kirk, J.N. Chapman, S. McVitie, P.R. Aitchison, C.D.W. Wilkinson, J. Appl. Phys. 87 (9) (2000) 5105.
[3] J. Yu, U. Rudiger, A.D. Kent, L. Thomas, S.S.P. Parkin, Phys. Rev., B 60 (10) (1999) 7352.
[4] J. Yu, U. Rudiger, L. Thomas, S.S. Parkin, A.D. Kent, J. Appl. Phys. 85 (8) (1999) 5501.
[5] R. Pulwey, M. Zolfl, G. Bayreuther, D. Weiss, J. Appl. Phys. 91 (10) (2002) 7995.
[6] P. Vavassori, V. Metlushko, M. Grimsditch, B. Ilic, P. Neuzil, R. Kumar, Phys. Rev., B 61 (9) (2000) 5895.
[7] M. Grimsditch, Y. Jaccard, I.K. Schuller, Phys. Rev., B 58 (17) (1998) 11539.
[8] D. Grujicic, B. Pesic, J. Magn. Magn. Mater. 285 (2005) 303.
[9] J. Shi, J. Li, S. Tehrani, J. App. Phys. 91 (10) (2002) 7458.
[10] D. Grujicic, B. Pesic, J. Magn. Magn. Mater. 288 (2005) 196.
[11] R. Naik, C. Kota, J.S. Payson, G.L. Dunifer, Phys. Rev., B 48 (2) (1993) 1008.
[12] S.D. Healy, K.R. Heim, Z.J. Yang, G.G. Hembree, J.S. Drucker, M.R. Scheinfein, J. Appl. Phys. 75 (10) (1994) 5592.
[13] S. Muller, P. Bayer, C. Reischl, K. Heinz, B. Feldmann, H. Zillgen, M. Wuttig, Phys. Rev. Lett. 74 (5) (1995) 765.
[14] B.D. Cullity, Introduction to Magnetic Materials, Pearson Addison Wesley, Boston, MA, 1972, p. 614.
[15] A. Robinson, W. Schwarzacher, J. Appl. Phys. 93 (2003) 7250.
[16] M.S. Wei, S.Y. Chou, J. Appl. Phys. 76 (1994) 6679.
[17] M. Grimsditch, Y. Jaccard, I.K. Schuller, Phys. Rev. (1998) 11539.
[18] M. Natali, A. Lebib, Y. Chen, I.L. Prejbeanu, K. Ounadjela, J. Appl. Phys. 91 (2002) 7041.
[19] Y. Hao, F.J. Castano, C.A. Ross, B. Vogeli, M.E. Walsh, H.I. Smith, J. Appl. Phys. 91 (2002) 7989.
[20] M.J. Donahue, D.G. Porter, OOMMF user's guide, version 1.0, interagency report NISTIR 6376, National Institute of Standards and Technology, Gaithersburg, MD, September 1999 (http://math.nist.gov/oommf/).
[21] M. Schneider, St. Muller-Pfeiffer, W. Zinn, J. Appl. Phys. 79 (11) (1996) 8578.